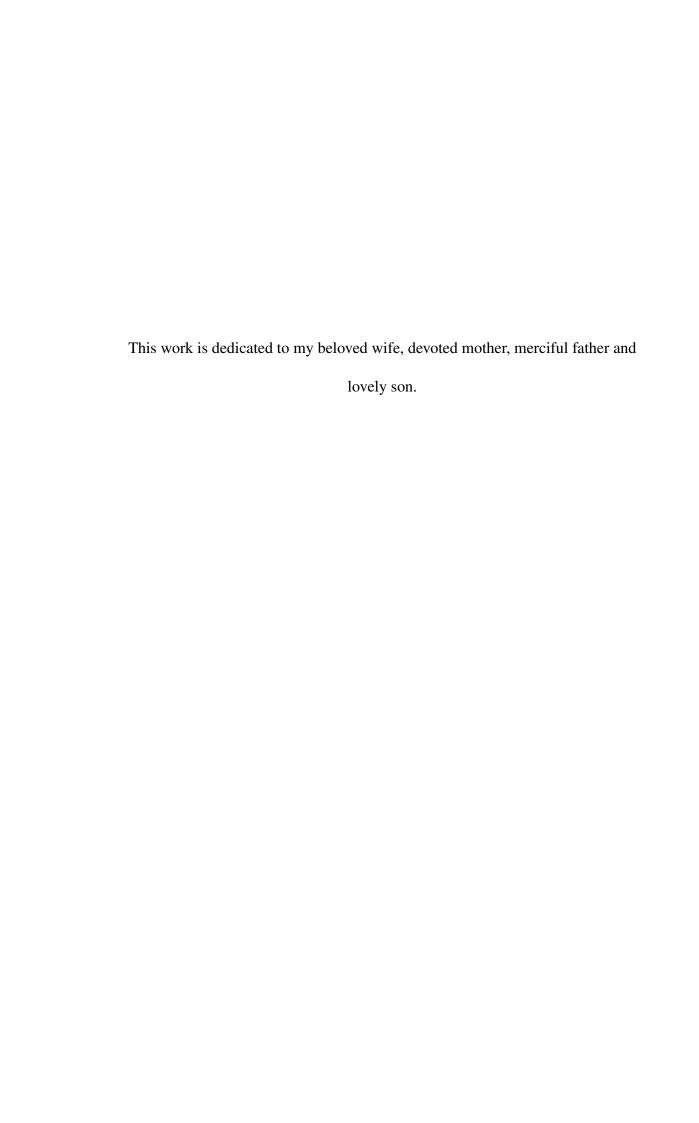
# DESIGN AND MODELING OF QUASI-LUMPED PLANAR INVERTED-F ANTENNA FOR HANDHELD DEVICES

## **MAJID RAFIEE**

## UNIVERSITI SAINS MALAYSIA



## DESIGN AND MODELING OF QUASI-LUMPED PLANAR INVERTED-F ANTENNA FOR HANDHELD DEVICES

by

**MAJID RAFIEE** 

Thesis submitted in fulfillment of the requirements for the degree of Doctor of Philosophy

February 2016

#### **ACKNOWLEDGEMENTS**

First and foremost, praise be to God, the most gracious and the most merciful. Without His blessing and guidance my accomplishments would never have been possible. I would like to express my deepest gratitude to my advisor, Dr. Aftanasar bin Md. Shahar and co-supervisor, Professor Dr. Mohd Fadzil Ain for their excellent guidance, caring, patience, and providing me with an excellent atmosphere for doing research. I could not have imagined having better advisors and mentors for my Ph.D study. Dr. Aftanasar bin Md. Shahar has this potential to devise a research topic with feasible foreseeable future results output. I sincerely desire his extent of patience and attributes of not given up on a student even in a hopeless situation until he turns them to a success story. He has demonstrated this attribute a number of times. He responds to questions, discussion, and review of write-ups either article or thesis almost instantly. Professor Dr. Mohd Fadzil Ain is not different either. He has a sense of humor that naturally dissipates and diffuses your pressure and stress in no time as you discuss the challenges of your work with him with much concern. They are simply amazing and good compliments.

I am greatly indebted to my wife, Farnaz Afkhami Aghda. As soon as I left Iran, you single handedly took up the challenges of taking over my responsibilities, first to you, my child, and finally, my parents. This I cannot thank you enough. I also want to thank my son, Ryan. I truly know how it feels to miss ones parents particularly at that formative years-Thank you! I specially want to thank my parents. With attainment of this degree, I perceived I have adequately fulfills my mum's dream toward my education.

I would like to express many thanks to all of the School Electrical and Electronic

Engineering office staffs, particularly, Mrs. Normala Omar and Mr. Mohd Rahmat Bin Arifin for their invaluable help during my study.

My sincere thanks also goes to technicians; Mr. Abdul Latip Hamid, Mr Elias Zainuddin and Mdm Zammira Khairuddin for their assistance and providing technical support in the Communications and PCB laboratory. I would like also to thank Universiti Sains Malaysia (USM), Institute of Postgraduate Studies (IPS) and School of Electrical & Electronics for providing the opportunity and supporting my research project through USM fellowship award and Teaching and Learning Assistant scheme (T&L) and Grants under project numbers 1001/PELECT/814202 USM RUT and 1001/PELECT/854004 USM RUT.

## TABLE OF CONTENTS

Ackr	owledg	ements	ii
Table	e of Cor	itents	iv
List	of Table	s	хi
List	of Figur	es	xiii
List	of Plate	s x	xiv
List	of Abbr	eviations	XXV
List	of Symb	pols x	xxi
Abst	rak	xx	xiv
Abst	ract	xx	xvi
СНА	PTER 1	– INTRODUCTION	
1.1		round	1
1.2		m statement	4
1.3		and Objectives	7
1.4		of Research	8
1.5		itions of Research	9
1.6	Thesis	Contribution	9
1.7		Outline	10
CHA	PTER 2	2 – LITERATURE REVIEW	
2.1	Introd	uction	13
2.2	Theore	etical Background	14
	2.2.1	Long Term Evolution (LTE)-Advanced Evolution Review	14
	2.2.2	Review of More Conventional Mobile Antennas in the Market	15
		2.2.2(a) Antenna Prerequisites to Be Used as a Mobile Antenna.	15
		2.2.2(b) Planar Inverted-F Antenna (PIFA) Evolution as an Internal Antenna for Mobile Devices	17

		2.2.2(c)	Specific Absorption Ratio (SAR) Standard for Near-Body Antennas	23
	2.2.3		and Quasi-Lumped Elements Used in Microwave ions	26
2.3	Design	n Modeling	g of PIFA and Quasi-Lumped Elements	29
	2.3.1	PIFA Mo	odeling as a Radiating Element	29
	2.3.2	PIFA Mo	odeling as a Resonating Element	32
	2.3.3	PIFA Eq	uivalent Circuit Modeling	33
		2.3.3(a)	Input Current Calculation of a Single Band PIFA	36
		2.3.3(b)	Input Voltage Calculation of a Single Band PIFA	37
		2.3.3(c)	Input Impedance Calculation of a Single Band PIFA	38
		2.3.3(d)	Analyzing of Shorting Pin in PIFA	40
	2.3.4	Quasi-Lu	imped Elements Modeling	42
		2.3.4(a)	Equivalent Circuit Modeling of a Parasitic Capacitor	44
		2.3.4(b)	Equivalent Circuit Modeling of an Interdigital Capacitor	47
		2.3.4(c)	Equivalent Circuit Modeling of a Quasi-Inductor	57
2.4	Conve	ntional PI	FA Antennas	60
	2.4.1	Conventi	onal PIFA Antennas Feeding Structure	60
	2.4.2	Conventi	onal single element PIFA antenna	60
	2.4.3	Conventi	onal PIFA Antennas as a MIMO Antenna	62
		2.4.3(a)	Effect of Spatial Diversity on Correlation in MIMO Configuration	63
		2.4.3(b)	Effect of Patten Diversity on Correlation in MIMO Configuration	63
		2.4.3(c)	Effect of Polarization Diversity on Correlation in MIMO Configuration	64
2.5	Summ	ary		65
СНА	PTER 3	B – METH	IODOLOGY	
3.1	Introdu	uction		66

3.2		neters and Design Principles of CPW-Fed Quasi-Lumped PIFA ina
	3.2.1	The Principle of the Feeding Structure
	3.2.2	Quasi-Lumped Elements Configuration Parameters of quasi-lumped PIFA.
3.3	Capac	citors of Proposed CPW-Fed Quasi-Lumped PIFA Antenna
	3.3.1	Capacitance of Parasitic Capacitor, $C_P$
		3.3.1(a) Charge per Unit on the Connected Narrow Transmission $Line(Q')$
		3.3.1(b) Total Charge on the Conductor $(Q_{total})$
	3.3.2	Open Stub Capacitance Calculation Using Wheeler Approach, $C_{OS}$
	3.3.3	Interdigital Capacitor( $C_I$ ) Calculation Using Conformal Mapping Technique
		3.3.3(a) Inherent Associated Resistance by Interdigital Capacitor (IDC)'s Conductor (Loss Through Conductor Sheet)
		3.3.3(b) Inherent Associated Inductance by IDC(produced by Fingers Length)
3.4	Induct	tors of Proposed CPW-Fed Quasi-Lumped PIFA Antenna
	3.4.1	Open Stub Inductance, $L_{OS}$ Using Wheeler's Approach
	3.4.2	Short-Circuited Inductor Calculation ( $L_{SC}$ ), Using Conformal Mapping Technique
3.5	Equiv	alent Circuit Modeling of CPW-Fed Quasi-Lumped PIFA Antenna .
3.6	Reson	nant Frequency of CPW-Fed Quasi-Lumepd PIFA Antenna
3.7	Dual I	Elements CPW-Fed Quasi-Lumped PIFA MIMO Antenna
3.8	Anten	ana Simulation using ADS and 3D microwave softwares
	3.8.1	Configuration of Simulation Softwares for CPW-Fed Quasi-Lupmed PIFA Antenna
	3.8.2	Defining of Dielectric Substrate Material
	3.8.3	Setting of Microstrip Feeder Impedance
	3.8.4	Defining of Waveguide Port

	3.8.5	Defining of Boundary Conditions	103
	3.8.6	Settings for Far-Field Monitor	103
	3.8.7	Transient Solver as the Main Solver in CST	104
	3.8.8	Impedance Calculator Toolbox	104
	3.8.9	Specific Absorption Ratio (SAR)	105
	3.8.10	Total Active Reflection Coefficient (TARC) Calculation for CPW-Fed Quasi-Lupmed PIFA MIMO Antenna	106
	3.8.11	Mean Effective Gain (MEG) Calculation for CPW-Fed Quasi-Lupmed PIFA MIMO Antenna	106
	3.8.12	Diversity Gain (DG) Calculation for CPW-Fed Quasi-Lupmed PIFA MIMO Antenna	110
3.9	Measu	rements Setup of CPW-Fed Quasi-Lupmed PIFA Antenna	110
	3.9.1	S-Parameter Measurement Setup	110
	3.9.2	Antenna Radiation Pattern Measurement Setup	111
	3.9.3	Gain Measurement Procedure	113
	3.9.4	Envelop Correlation Coefficient (ECC) Calculation	115
	3.9.5	Mean Effective Gain (MEG) Calculation	119
	3.9.6	Total Active Reflection Coefficient (TARC) Calculation	121
3.10	Summa	ary	122
СНА	PTER 4	– PARAMETRIC DISCUSSION	
4.1	-	lent Circuit Model of Single Element CPW-Fed Quasi-Lumped Antenna Using Advanced Design System (ADS)	124
4.2	Effect	of Open Stub on Antenna's Frequency and Bandwidth	129
	4.2.1	Effects of Open Stub capacitance $(C_{OS})$ Variations on Quasi-Lumped PIFA Antenna's Operating Frequency and Bandwidth	129
	4.2.2	Effects of Open Stub Inductance ( $L_{OS}$ ) Variations on Quasi-Lumped PIFA Antenna's Operating Frequency and Bandwidth	130
	4.2.3	Summary on the Effect of Open Stub on the Antenna Performance	132

4.3	Variati	ions on Qu	uasi-Lumped PIFA Antenna's Operating Frequency and	135
	4.3.1		of Series Inductance ( $L_{Series}$ ) variations on Quasi-Lumped operating Frequency and Bandwidth	135
	4.3.2		of Series Resistance ( $R_{Series}$ ) variations on Quasi-Lumped operating Frequency and Bandwidth	136
	4.3.3	Quasi-Lu	of Interdigitated Capacitance $(C_I)$ Variations on amped PIFA Antenna's Operating Frequency and lth	136
	4.3.4	Summar	y on the effect of using IDC	140
4.4			tic Capacitance $(C_P)$ Variations on Quasi-Lumped PIFA ating Frequency and Bandwidth	140
4.5			Circuited Inductance ( $L_{SC}$ ) Variations on Quasi-Lumped Operating Frequency and Bandwidth	142
4.6	Summ	ary		143
СНА	APTER 5	5 – RESU	LTS AND DISCUSSION	
5.1	Introd	uction		144
5.2	Model	ling, Simu	lation and Measurement Results	144
	5.2.1	_	gle-Element CPW-Fed Quasi-Lumped PIFA Antenna ration	144
		5.2.1(a)	Modeled, Simulated and Measured Reflection Coefficient of Single-Element Quasi-Lumped PIFA	145
		5.2.1(b)	Simulated Smith Chart of Single-Element CPW-Fed Quasi-Lumped PIFA Antenna	148
		5.2.1(c)	Modeled, Simulated and Measured Voltage Standing Wave Ratio (VSWR) of Single-Element Quasi-Lumped PIFA	149
		5.2.1(d)	Modeled, Simulated and Measured Mismatch Loss (ML) of Single Element Quasi-Lumped PIFA	149
		5.2.1(e)	Simulated and Measured Radiation Pattern of Single Element CPW-Fed Quasi-Lumped PIFA Antenna	151
		5.2.1(f)	Simulated Surface Current Distribution of Single Element Quasi-Lumped PIFA	153

		5.2.1(g)	Simulated and Measured Gain of Single Element CPW-Fed Quasi-Lumped PIFA Antenna	155
		5.2.1(h)	Simulated Specific Absorption Ratio (SAR) of Single Element Quasi-Lumped PIFA Antenna	156
	5.2.2		l-Element CPW-Fed Quasi-Lumped PIFA MIMO Configuration	160
		5.2.2(a)	Equivalent Circuit Model of Dual-Element CPW-Fed Quasi-Lumped PIFA MIMO Antenna Using Advanced Design System (ADS)	160
		5.2.2(b)	Modeled, Simulated and Measured Reflection Coefficient And Mutual Coupling of Dual-Element CPW-Fed Quasi-Lumped PIFA MIMO Antenna	162
		5.2.2(c)	Modeled, Simulated and Measured Voltage Standing Wave Ratio (VSWR) of Dual-Element Quasi-Lumped PIFA MIMO Antenna	165
		5.2.2(d)	Modeled, Simulated and Measured Mismatch Loss (ML) of Dual-Element Quasi-Lumped PIFA MIMO Antenna	166
		5.2.2(e)	Simulated and Measured Radiation Pattern of Dual-Element Quasi-Lumped PIFA MIMO Antenna	168
		5.2.2(f)	Simulated Current Surface of Dual-Element Quasi-Lumped PIFA MIMO Antenna	168
		5.2.2(g)	Simulated Specific Absorption Ratio (SAR) of Dual-Element Quasi-Lumped PIFA MIMO Antenna at Its Operating Frequency	170
		5.2.2(h)	Modeled, Simulated and Measured Total Active Reflection Coefficient (TARC) of Dual-Element Quasi-Lumped PIFA MIMO Antenna	171
		5.2.2(i)	Modeled, Simulated and Measured Envelop Correlation Coefficient (ECC) of Dual-Element Quasi-Lumped PIFA MIMO Antenna	173
		5.2.2(j)	Simulated Mean Effective Gain (MEG) of Dual-Element Quasi-Lumped PIFA MIMO Antenna	174
		5.2.2(k)	Modeled, Simulated and Measured Diversity Gain (DG) of Dual-Element Quasi-Lumped PIFA MIMO Antenna	175
5.3	_		Proposed Quasi-Lumped PIFA Antenna With FA Antennas	176

	5.3.1	Comparison of Single-Element CPW-Fed Quasi-Lumped PIFA Antenna With Conventional PIFA Antennas	176
	5.3.2	Comparison of Dual-Element Quasi-Lumped PIFA MIMO Antenna With Conventional PIFA Antennas	176
5.4	Summ	ary	179
СНА	PTER 6	6 – CONCLUSION AND FUTURE WORK	
6.1	Conclu	usion	180
6.2	Sugges	stions for future works	185
	6.2.1	Modification for other devices	185
	6.2.2	Higher order of MIMO antenna	185
	6.2.3	Multi-frequency	186
	6.2.4	Next Generation Systems and Other Devices	186
REFI	ERENC	ES	188
APPI	ENDICI	ES	
LIST	OF PU	BLICATIONS	

## LIST OF TABLES

		Page
Table 2.1	Minimum requirements assigned for mobile antennas (Stutzman and Thiele, 2012a)	17
Table 2.2	Lumped Elements Categories	27
Table 2.3	Definition of assumed parameters used in applied radiating and balanced mode theory on a conventional single band PIFA	37
Table 2.4	Ports roles shown in Figure 2.18 for analyzing short pin and slot	39
Table 2.5	Recent researches on PIFA and MIMO configuration	64
Table 3.1	Design specifications thresholds to design CPW-fed quasi-lumped PIFA antenna to be used as a cellphone antenna	68
Table 3.2	$d_{j,i}$ value calculation considering Figure 3.13	90
Table 3.3	Component representation for equivalent circuit model of CPW-fed quasi-lupmed PIFA antenna	97
Table 3.4	Propagation scenarios used to evaluate the performance of the antenna systems (Karaboikis et al., 2008; Plicanic, 2004)	109
Table 4.1	Initial parameters' value of proposed quasi-lumped PIFA antenna	126
Table 4.2	initial calculated values of component used in equivalent circuit model and their related equations	126
Table 5.1	Optimized parameters' dimension and components' value of proposed CPW-fed quasi-lumped PIFA antenna	145
Table 5.2	Comparison of Return Loss (RL) results for modeled, simulated and measured of 2.6 GHz	147
Table 5.3	Comparison VSWR return loss value for modeled, simulated (using CST and HFSS) and measured of single element CPW-fed quasi-lumped PIFA antenna at frequency of 2.6 GHz	150
Table 5.4	Comparison of modeled, simulated (using CST and HFSS) and measured reflected loss of single element CPW-fed quasi-lumped PIFA antenna representing at operation frequency of 2.6 GHz and the frequency with lowest mismatch loss	151

Table 5.5	Comparison of simulated (using CST and HFSS) and measured antenna gain of single element CPW-fed quasi-lumped PIFA antenna at different frequencies	157
Table 5.6	Peak value of SAR at a point, standard peak average masses and fixed volume mass for single element CPW-fed quasi-lumped PIFA antenna at operating frequency (2.6 GHz)	157
Table 5.7	Assigned properties (permittivity $(\varepsilon_r)$ and conductivity $(\sigma)$ to simulate the head SAM-phantom model including tissue and vessels	159
Table 5.8	Comparison of modeled, simulated (using CST and HFSS) and measured return loss at 2.6 GHz for dual-element CPW-fed quasi-lumped PIFA MIMO antenna	164
Table 5.9	Comparison modeled, simulated (using CST and HFSS) and measured mutual coupling (S12 & S21) of 2.6 GHz for dual-element CPW-fed quasi-lumped PIFA MIMO antenna	164
Table 5.10	Comparison of modeled, simulated (using CST and HFSS) and measured VSWR of 2.6 GHz	165
Table 5.11	Comparison of modeled, simulated (using CST and HFSS) and measured Mismatch Loss (ML) of dual-element CPW-fed quasi-lumped PIFA MIMO antenna showing at operating frequency (2.6 GHz) and the frequency with minimum reflected loss	167
Table A.1	System performance requirements for acIMT- & LTE- Advanced	
Table B.1	Mobile cellphones evolutions	
Table C.1	Equations for effective external inductance, as found in literature	

## LIST OF FIGURES

		Page
Figure 2.1	A comparison of the electric field distributions	18
Figure 2.2	Evolution of Inverted-F Antenna (IFA) and Planar Inverted-F Antenna (PIFA)	19
Figure 2.2(a)	Conventional monopole antenna	19
Figure 2.2(b)	50-ohm matched monopole antenna	19
Figure 2.2(c)	L-shaped antenna	19
Figure 2.2(d)	IFA (or a PIFA side view)	19
Figure 2.3	Palm antennas locating on back of the cellphone (Bevelacqua, n.d.)	19
Figure 2.4	Half-wavelength patch with shorting pin at the feed	20
Figure 2.5	Quarter-wavelength Patch side view	20
Figure 2.6	Current and voltage at microstrip patch antenna. It shows the voltage is zore at middle of patch and current is in its peak since voltage and current are out phase.	21
Figure 2.7	Overall input impedance of a PIFA antenna	22
Figure 2.8	The effect of shorting posts numbers and position on PIFA	23
Figure 2.9	The evolution and performance of GSM antenna types from 1995 to 2011	24
Figure 2.10	Current and Three Dimensional (3D) radiation pattern of a PIFA operating at 1.8 GHz	25
Figure 2.11	3D radiation pattern and surface current distribution od Planar Monopole Antenna (PMA) operating at 1.9 GHz	25
Figure 2.12	PIFA in real markets	26
Figure 2.13	PIFA configuration and radiating magnetic current on different paths	30
Figure 2.14	Perspective view of a conventional 3D PIFA antenna showing shorting post (pin) and feeder location	32
Figure 2.15	Single band Planar Inverted-F Antenna	34

Figure 2.16	Radiating and Balanced mode analysis of PIFA with a loaded unfed pin	34
Figure 2.17	Simplified radiating and balanced mode analysis of PIFA shorting pin	36
Figure 2.18	Dual frequencies PIFA	40
Figure 2.19	Dual-band PIFA equivalent circuit	41
Figure 2.20	Simplified dual-band PIFA equivalent circuit	42
Figure 2.21	Perspective view of Interdigital Capacitor (IDC)	48
Figure 2.22	The Interdigital Capacitor (IDC) and its subcomponents	49
Figure 2.23	Equivalent circuit of Interdigital Capacitor in low frequency proposed by Alley (1970)	50
Figure 2.24	Improvement and verification of Equivalent Circuit of IDC offered by Alley by Wolff and Kibuuka (1984)	51
Figure 2.25	Equivalent circuit of interdigital capacitor derived by Pattenpaul et al. (1988) in (a) Series and (b) shunt representation	51
Figure 2.25(a)	Series EC element	51
Figure 2.25(b)	Shunt EC element	51
Figure 2.26	Equivalent Circuit of interdigital capacitor derived by Bahl (2003) at (a) low frequency and (b) high frequency	52
Figure 2.26(a)	Low frequency equivalent circuit element	52
Figure 2.26(b)	High frequency equivalent circuit element	52
Figure 2.27	The value of $A_1$ and $A_2$	53
Figure 2.28	Representation of a flat inductor in perspective view	58
Figure 3.1	Flow chart showing research methodology for designing CPW-fed quasi-lumped PIFA antenna in single- and dual-element MIMO Configuration	67
Figure 3.2	Modeling flow chart in detail	69
Figure 3.2(a)	General procedure of modeling	69
Figure 3.2(b)	Modeling procedure of parasitic capacitor	69
Figure 3.2(c)	Modeling procedure of IDC	69

Figure 3.3	Representation of voltage allocation through microstrip feed line	70
Figure 3.4	Representation of physical parameters of proposed antenna	71
Figure 3.5	CPW-fed quasi-lumped PIFA antenna subcomponents	72
Figure 3.6	Charge calculation for parasitic capacitance calculation	73
Figure 3.7	The equivalent capacitance produced by $C_P$ with the reference to $X_1$ , $X_2$ , $Y/2$ and $Z$ are in $mm$ and are defined as the distances to the front, lateral electric walls, magnetic wall and to the upper surface, respectively	79
Figure 3.8	Cross view of interdigital capacitance fingers and short-circuited inductor assuming the distance between all elements is equal	80
Figure 3.9	Cross section view of interdigital capacitor's fingers to show how patch CDEF is mapped to path C'D'E'F' using Schwarz-Christoffel transformation	81
Figure 3.10	Cross section view of inductor and interdigital capacitor's fingers with unequal separation distance	85
Figure 3.11	Assumed voltages $(V_{ext}, V_1 \text{ and } V_2)$ , current $(\frac{I_0}{2n})$ and capacitor fingers positions for inductance calculation. Current in all figures is assumed to be equal because of having symmetrical structure	86
Figure 3.12	Cross-section showing magnetic fluxes $\Phi_1$ , $\Phi_2$ and $\Phi_3$ for a current, $I_0$ flowing in the leftmost strip (center strip in Figure 3.11 with unequal gaps between fingers and inductor)	87
Figure 3.13	Cross-section showing equal gaps between inductor and IDC fingers magnetic fluxes	89
Figure 3.13(a)	Equal gaps between inductor and IDC fingers	89
Figure 3.13(b)	magnetic fluxes $\Phi_1, \Phi_2$ and $\Phi_3$ for a current, $I_0$	89
Figure 3.14	Variation of input impedance along the open/short-circuited	94
Figure 3.14(a)	Variation of input impedance along open-circuited	94
Figure 3.14(b)	Variation of input impedance along the short-circuited	94
Figure 3.15	Input impedance for different wavelengths of open/short-circuited line	95
Figure 3.15(a)	Input impedance for different wavelengths of open-circuited line	95
Figure 3.15(b)	Input impedance for different wavelengths of short-circuited line	95

Figure 3.16	antenna at high frequency over a wide bandwidth (I) short circuit, (II) interdigital and parasitic capacitors, (III) PCB contribution and (IV) open stub capacitor and inductor	96
Figure 3.17	Equivalent circuit model of the CPW-fed quasi-lumped PIFA antenna in a narrow bandwidth where PCB contribution can be ignored	97
Figure 3.18	Equivalent circuit of CPW-fed quasi-lumped PIFA antenna over a narrow bandwidth considering the point that the second pad capacitor of IDC is grounded.	98
Figure 3.19	Top view of CPW-fed quasi-lumped PIFA MIMO antenna with dual elements array configuration and spatial diversity technique where two elements are placed at a distance more than half-wavelength	100
Figure 3.20	Equivalent circuit model of CPW-fed quasi-lumped PIFA antenna in MIMO configuration with dual elements array over a narrow bandwidth	100
Figure 3.21	Simulation of proposed antenna in (a) CST and (b) HFSS environment	105
Figure 3.21(a)	Simulation of proposed antenna in CST	105
Figure 3.21(b)	Simulation of proposed antenna in HFSS environment	105
Figure 3.22	Schematic view of proposed antenna integrated in phase shifter circuit using CST Design Studio to simulate TARC	107
Figure 3.23	Gain measurement setup to measure gain of AUT by comparing it with a standard antenna as a reference	114
Figure 4.1	Quasi-lumped PIFA antenna geometry and model	124
Figure 4.1(a)	Parametric dimensions on design	124
Figure 4.1(b)	Parametric components on model	124
Figure 4.2	Flow chart showing the work flow of parametric study on modeled and simulated antenna	125
Figure 4.3	Equivalent circuit of single element quasi-lumped PIFA modeled in ADS with predefined variables used for parametric study of modeled results	128
Figure 4.4	Value of $C_{OS}$ versus $W_S$ and $D_S$	129
Figure 4.4(a)	Value of $C_{OS}$ versus $W_S$	129

Figure 4.4(b)	Value of $C_{OS}$ versus $D_S$	129
Figure 4.5	Sweeping return loss results according to their initial values obtained in Table 4.2 and 4.1. The best value can be achieved with regard to minimum specifications mentioned in Table 3.1(a) Modeled return loss by varying open stub capacitance $(C_{OS})$ using ADS, (b) simulated return loss by varying $W_S$ and $D_S$ using CST (c) simulated return loss by varying $W_S$ and $D_S$ using HFSS	131
Figure 4.5(a)	Modeled return loss versuse $C_{OS}$	131
Figure 4.5(b)	Simulated return lost using CST versus $W_S$	131
Figure 4.5(c)	Simulated return loss using HFSS versus $W_S$	131
Figure 4.6	Value of $L_{OS}$ versus $W_S$ and $D_S$	132
Figure 4.6(a)	Value of $L_{OS}$ versus $W_S$	132
Figure 4.6(b)	Value of $L_{OS}$ versus $D_S$	132
Figure 4.7	Modeled and simulated return loss by varying inductance $L_{OS}$ , width $W_S$ and length $L_S$	133
Figure 4.7(a)	Modeled return loss versus $L_{OS}$	133
Figure 4.7(b)	Simulated return loss versus $L_{OS}$ and $W_S$ using CST	133
Figure 4.7(c)	Simulated return loss versus $L_{OS}$ and $W_S$ using HFSS	133
Figure 4.8	The variation of series inductance and resistance versus IDC's length	135
Figure 4.9	The variation of series resistance versus IDC's length and width	136
Figure 4.9(a)	The variation of series IDC resitance versus $L_C$	136
Figure 4.9(b)	The variation of series IDC resistance versus $W_C$	136
Figure 4.10	Variation of $C_I$ versus $W_C$ and $L_C$	137
Figure 4.10(a)	Variation of $C_I$ versus $L_C$	137
Figure 4.10(b)	Variation of $C_I$ versus $W_C$	137
Figure 4.11	Modeled reflection coefficient variation versus IDC dimensions	138
Figure 4.11(a)	Modeled reflection coefficient variation versus IDC dimensions $L_C$	138
Figure 4.11(b)	Modeled reflection coefficient variation versus $W_C$	138

Figure 4.12	Sweeping simulated return loss results using CST versus IDC's length, $L_C$ and width, $W_C$	139
Figure 4.12(a)	Simulated reflection coefficient variation versus $L_C$ using CST	139
Figure 4.12(b)	Simulated reflection coefficient variation versus $W_C$ using CST	139
Figure 4.13	The simulated (HFSS) reflection coefficient variations versus IDC's length and width	141
Figure 4.13(a)	Simulated reflection coefficient variation versus $L_C$ using HFSS.	141
Figure 4.13(b)	Simulated reflection coefficient variation versus $W_C$ using HFSS	141
Figure 4.14	The variation of reflection coefficient versus parasitic capacitance, $C_P$	142
Figure 4.15	The variation of reflection coefficient versus parasitic capacitance, $C_P$	143
Figure 5.1	The geometry and parametric dimensions of the printed CPW-fed quasi-lumped PIFA antenna	145
Figure 5.2	Equivalent circuit model of single element CPW-fed quasi-lumped PIFA antenna in ADS	146
Figure 5.3	Comparison of modeled. simulated (using CST and HFSS) and measured return loss of single element CPW-fed quasi-lumped PIFA antenna	148
Figure 5.4	Simulated input impedance of CPW-fed quasi-lumped PIFA antenna at operating frequency	149
Figure 5.5	Comparison of modeled, simulated (using CST and HFSS) and measured VSWR of single element CPW-fed quasi-lumped PIFA antenna	150
Figure 5.6	Simulated and measured radiation pattern of single element CPW-fed quasi-lumped PIFA antenna at operation frequency of 2.6 GHz showing at (a) E-Plane and (b) H-Plane	152
Figure 5.6(a)	Simulated and measured radiation pattern for E-Plane	152
Figure 5.6(b)	Simulated and measured radiation pattern for H-Plane	152
Figure 5.7	Surface current of CPW-fed quasi-lumped PIFA antenna showing at its resonant frequency. Current density is maximum near the shorting strip and becomes lower at resonator's far edges.	155

Figure 5.8	of single element CPW-fed quasi-lumped PIFA antenna. The minimum considered gain by handsets specifications mentioned in Table 3.1 is achieved at operating frequency (2.6 GHz)	156
Figure 5.9	Simulated SAR in average mass of 1 gram (US standard) for single element quasi-lumped PIFA antenna showing at (a) perspective (b) top and (c) front view	158
Figure 5.9(a)	SAR perspective view for US standard	158
Figure 5.9(b)	SAR top view for US standard	158
Figure 5.9(c)	SAR front view for US standard	158
Figure 5.10	Simulated SAR in average mass of 10 grams (EU standard) for single element quasi-lumped PIFA antenna showing at (a) perspective (b) top and (c) front view	158
Figure 5.10(a)	SAR perspective view for EU standard	158
Figure 5.10(b)	SAR top view for EU standard	158
Figure 5.10(c)	SAR front view for EU standard	158
Figure 5.11	Dual-element MIMO prototype	160
Figure 5.12	Equivalent circuit modeling of the dual-element Coplanar Waveguide (CPW)-fed quasi-lumped quasi-PIFA MIMO antenna represented in ADS. The model is shown for a MIMO spatial diversity position where two elements were placed symmetrically with a proper distance	161
Figure 5.13	Modeled, simulated and measured return loss at 2.6 GHz	163
Figure 5.13(a)	Modeled, simulated and measured return loss at 2.6 GHz for first element	163
Figure 5.13(b)	Modeled, simulated and measured return loss at 2.6 GHz for second element	163
Figure 5.14	VSWR for modeled, simulated and measured antenna in MIMO configuration	166
Figure 5.14(a)	VSWR for modeled, simulated and measured antenna in MIMO configuration for first element	166
Figure 5.14(b)	VSWR for modeled, simulated and measured antenna in MIMO configuration for second element	166
Figure 5.15	Simulated and measured radiation pattern for proposed Multi Input Multi Output (MIMO) antenna	168

Figure 5.15(a)	antenna E-plane	168
Figure 5.15(b)	Simulated and measured radiation pattern for proposed MIMO antenna H-plane	16
Figure 5.16	Surface current of proposed antenna in MIMO configuration	169
Figure 5.16(a)	Surface current of proposed antenna in MIMO configuration for first element	169
Figure 5.16(b)	Surface current of proposed antenna in MIMO configuration for second element	16
Figure 5.17	Simulated SAR in average mass of 1 gram (US standard) of PIFA MIMO antenna	17
Figure 5.17(a)	Simulated SAR in average mass of 1 gram (US standard) perspective view	17
Figure 5.17(b)	Simulated SAR in average mass of 1 gram (US standard) top view	17
Figure 5.17(c)	Simulated SAR in average mass of 1 gram (US standard) front view	17
Figure 5.18	Simulated SAR in average mass of 10 gram (EU standard) for PIFA MIMO antenna (a) perspective (b) top and (c) front view	17
Figure 5.18(a)	Simulated SAR in average mass of 10 gram (EU standard) perspective view	17
Figure 5.18(b)	Simulated SAR in average mass of 10 gram (EU standard) top view	17
Figure 5.18(c)	Simulated SAR in average mass of 10 gram (EU standard) front view	17
Figure 5.19	TARC for proposed MIMO antenna	17
Figure 5.19(a)	Modeled TARC for proposed MIMO antenna	17
Figure 5.19(b)	Simulated (CST) TARC for proposed MIMO antenna	17
Figure 5.19(c)	Simulated (HFSS) TARC for proposed MIMO antenna	17
Figure 5.19(d)	Mesured TARC for proposed MIMO antenna	17
Figure 5.19(e)	comparison of modeling, simulated and measured results	17

Figure 5.20	Comparison of modeled, simulated (CST and HFSS) and measured Envelop Correlation Coefficient (ECC) for dual-element CPW-fed quasi-lumped PIFA MIMO antenna	174
Figure 5.21	Modeled, simulated (CST and HFSS) and measured Diversity Gain (DG) of dual-element CPW-fed quasi-lumped PIFA MIMO antenna	175
Figure 5.22	Comparison of measured return loss for a single element CPW-fed quasi-lumped PIFA antenna with a conventional PIFA antenna presented by Gao et al. (2007a)	177
Figure 5.23	Comparison of measured s-parameters of a dual-element CPW-fed quasi-lumped PIFA MIMO antenna with a conventional dual-element PIFA MIMO antenna resented by Gao et al. (2007a) (a) s-parameters for first element (antenna 1) and (b) s-parameters for second element (antenna 2)	178
Figure A.1	Carrier aggregation (Ik Suh, 2011)	
Figure A.1(a)	Contiguous carrier aggregation	
Figure A.1(b)	Non-contiguous carrier aggregation	
Figure A.2	Carrier aggregation sample	
Figure A.3	Downlink CoMP transmission (Ghadialy, 2011)	
Figure A.3(a)	Coordinated beamforming/Coordinated schedualing	
Figure A.3(b)	Joint processing (Joint transmission)	
Figure A.3(c)	Joint processing (Dynamic cell selection)	
Figure A.4	Capacity Improvement (Lo and Niemegeers, 2009)	
Figure A.5	Amplify & Forward	
Figure A.6	Decode & Forward	
Figure C.1	IDCs types (Zhu and Wu, 2000; Emili et al., 2002)	
Figure C.1(a)	IDC type A	
Figure C.1(b)	IDC type B	
Figure C.1(c)	IDC type C	
Figure C.2	(a) Susceptance equivalent network representation and (b) J -inverter network equivalent representation (Zhu and Wu, 2000; Emili et al., 2002; Bahl, 2003)	

Figure C.2(a)	
Figure C.2(b)	
Figure C.3	2-D inductor types: (a) meander, (b) rectangular, (c) circular, and (d) octagonalBahl (2003).
Figure C.3(d)	listentry
Figure C.4	3-D inductor typesBahl (2003)
Figure C.4(a)	listentry
Figure C.4(b)	listentry
Figure C.5	The mutual inductance, M, in relation with the self-inductance, $L_1$ and $L_2$
Figure C.5(a)	subcaption
Figure C.5(b)	subcaption
Figure C.6	Self-, mutual- and effective- inductance
Figure C.7	Calculating $L_{self}$ , $M$ and $L_{eff}$ using the magnetic flux around the FGC.
Figure C.7(a)	$L_{self}$
Figure C.7(b)	<i>M</i>
Figure C.7(c)	$L_{eff}$
Figure C.8	Choice of axes
Figure C.8(a)	symmetric
Figure C.8(b)	asymmetric
Figure C.9	Rectangular loop, reprinted from (Paul, 1989)
Figure C.9(a)	The physical dimenssion
Figure C.9(b)	Equivalent circuit
Figure D.1	Cross section view showing conformal mapping applied on the inductor's cross section to map path ECEF to C'D'E'F' using Schwarz-Christoffelare mapping technique
Figure D.2	Cross section view of interdigital capacitor's fingers to show how patch CDEF is mapped to path C'D'E'F' using